

Performance-Oriented Design for Intelligent Reflecting Surface Assisted Federated Learning

Yapeng Zhao, Qingqing Wu, Wen Chen

Abstract—To efficiently exploit the massive raw data that is pervading generated at mobile edge networks, federated learning (FL) has emerged as a promising distributed learning technique that was regarded as a substitute for centralized learning operations. By collaboratively training a shared learning model at edge devices, the raw data transmission and storage are bypassed via the local computed parameters/gradients exchange in FL. Hence, FL can overcome high communication latency and privacy issues. While the high dimensionality in iterative updates (millions of parameters/gradients may be included in the model training) still conflicts with the scarcity of communication resources. Over-the-air computation (AirComp) has come into the spotlight recently which profitably leverages the inherent superposition property of wireless channels to perform efficient model aggregation. However, the model aggregation accuracy is still severely damaged by the unfavorable wireless propagation channels. In this paper, we harness the intelligent reflecting surface (IRS) to program the wireless channel, thus acquiring a satisfying learning performance. Specifically, a performance-oriented design scheme that directly minimizes the optimality gap of the loss function is proposed to accelerate the convergence of AirComp based FL. Firstly, we analyze the convergence behavior of the FL procedure. Then, both offline and online design approaches are proposed based on the obtained optimality gap. We adopt the block coordinate descent (BCD) method to tackle the highly-intractable problem. Simulation results demonstrate that such a performance-oriented design strategy can achieve higher test accuracy than the conventional isolated mean square error (MSE) minimization approach in FL.

Index Terms—Intelligent reflecting surface, over-the-air computation, federated learning, Lyapunov framework, transceiver design, passive beamforming.

I. INTRODUCTION

Recent years have witnessed a bloom of artificial intelligence (AI) applications throughout both industry and academia, such as image recognition and natural language processing. Moreover, some delay-sensitive applications like autonomous driving require timely processing of the generated enormous real-time data. Conventional approaches require a data center to collect all the raw data for centralized model training. While collecting massive amounts of data from distributed devices incurs high latency, huge energy and bandwidth cost [1]–[3]. Furthermore, the computation resources of edge devices are wasted and potential privacy violations exist since local data is collected and processed at the central server. Aiming to meet these urgent demands as aforementioned, the

emerging edge AI pushes the AI frontier from the network center to the edge, where the implicit knowledge was locally distilled to provide timely and economic intelligence as well as the privacy assurances. Chief among them is the thriving federated learning (FL) framework, in which local model parameters or gradients are exchanged instead of the raw data [4]–[6].

Since the training procedure in a state-of-the-art deep neural network (DNN) may involve millions of parameters [4], uplink communication overhead incurred during the iterative model update process is still a critical bottleneck. Besides, the communication bandwidth of participating edge devices is limited, and this situation is getting more severe especially when facing a large amount of devices. Hence, researchers are prompted to develop economic and communication-efficient uploading strategies to assist the FL procedure. Conventionally, edge devices are orthogonally allocated to upload their local model parameters/gradients, and the edge server sequentially decodes the received signals. While the required radio resources were greatly scaled with the number of participating devices and the model dimension in that case. Therefore, different strategies were proposed to alleviate the communication overhead with sacrificing moderate learning performance, e.g., device sampling based on the network topology [7], model sparsification [8] through the time correlations, gradient quantization via lossy compression [9] even only the sign of each stochastic gradient [10]. All the aforementioned schemes were shown as a concession with performance sacrificing due to the limited communication resources. Fortunately, the recently aroused over-the-air computation (AirComp) strategy has shown its efficiency in *one-shot* aggregation of the simultaneously transmitted local model parameters/gradients compared to the initial employed orthogonal multiple access (OMA) protocols [11], [12]. AirComp is a disruptive technology that turns the air into a computer by profitably leveraging the inherent waveform superposition property of wireless channel [12]. AirComp allows all the devices simultaneously access all the radio resources instead of only a fraction of them as in conventional OMA schemes, which significantly alleviates the bottleneck caused by limited communication resources. The idea of AirComp can be traced back to the pioneer works on studying functional computation in wireless sensor networks [13], and the computable function space can be extended from simple linear functions [14], [15] to arbitrary functions through nomographic decomposition [16], [17]. Besides, its *one-shot* function computation capability has been validated in a series of works, such as initial foundation elaboration from the information theory perspective [14], [15], [18], performance

Y. Zhao, and Q. Wu and are with the State Key Laboratory of Internet of Things for Smart City, University of Macau, Macao 999078, China (email: yc17435@connect.um.edu.mo; qingqingwu@um.edu.mo). W. Chen is with the Department of Electronic Engineering, Shanghai Jiao Tong University, Shanghai 200240, China (e-mail: wenchen@sjtu.edu.cn).

analysis for various systems from the signal processing perspective [19], [20], and prototype validation in the practical implementation [21], [22].

The initial AirComp based FL framework was proposed in [11], where AirComp was shown its substantial latency reduction compared to the orthogonal transmission. AirComp empowered FL system has been comprehensively investigated from various parts recently, primarily are how to accelerate the convergence of FL under tight resources constraints (e.g., communication and computation resources) [23] or reduce resources consumption with maintaining a satisfying learning performance [24]. Specifically, the design issues in prior works can be divided into two parts: one is the system optimization from the communication perspective containing device scheduling [25]–[27], transceiver design [28], [29], and parameters/gradients compressing [30], [31]; another is the inherent design of hyperparameters in the learning procedure, such as the learning rate [32] and batch size [33]. For example, the authors in [27] presented a two-step framework for joint device scheduling and receive beamformer design to achieve higher test accuracy. The local learning rate at edge devices was optimized in [32] to combat the distortion induced by the fading channel. Although AirComp has been envisioned and further validated to be a promising scalable model aggregation solution in FL, an intrinsic but fatal defect obstructs its implementation in practice. That is, the device with the worst channel dominates the overall aggregation error in AirComp based FL [19], [20], which is because the remaining devices with better channel qualities have to reduce their transmit power in order to perform precise signal alignment at the receiver. Hence, the strength of the obtained signal is diminished, and the aggregation accuracy is highly sensitive to the inherent noise. Therefore, the unfavorable propagation environment inevitably limits the performance of AirComp based FL. Fortunately, the recently emerging intelligent reflecting surface (IRS), a promising technology in the beyond fifth-generation (B5G) and the future sixth-generation (6G) network, overcomes this detrimental effect of channel fading via reconfiguring the wireless propagation environment [34]–[37]. By smartly tuning the signal reflection angle via a large number of low-cost passive reflecting elements, IRS is capable of dynamically altering wireless channels to a favorable one to guarantee a precise model aggregation procedure, thus enhancing the FL performance. Recent works have demonstrated the effectiveness of IRS in improving the test accuracy of FL, e.g., the authors in [27], [38] utilized the IRS to enhance the weak channel thus to involve more devices into collaborate model training. Moreover, multiple IRSs were adopted to further guard the model uploading phase [39].

The existing system design schemes in AirComp based FL are mainly focused on the separated mean square error (MSE) minimization in each communication round [11], [27], [38]. Although it seems reasonable since a more precise model uploading procedure makes the global model updates more accurate. But it is still a system optimization from the communication perspective, which isolates the communication phase from the learning phase. Notice that communication is served for model training during the entire FL procedure. While

the communication system design in the existing literature has not been tailored to the inherent characteristics of FL. Specifically, FL is a long-term process consisting of many progressive learning rounds that collectively determine the ultimate learning performance [40], [41]. Different learning rounds may have varying significance toward the convergence rate and the final model accuracy due to this intrinsic nature. Hence, resources need to be balanced among the iterations in FL via analyzing the collective impact of successive communication rounds on the ultimate performance. However, every learning rounds are treated equally in almost all the existing works, in which resources are isolated allocated across different learning rounds. Such an inappropriate system design invisibly results in a performance loss. Therefore, establishing a communication resource allocation policy in FL requires determining the learning efficiency of different communication rounds in advance.

In this paper, we consider the AirComp based FL system, in which an IRS was employed to configure a favorable wireless channel to provide precise model aggregation in each iteration. We propose a performance-oriented design approach to fully unleash the available communication resources, thus obtaining higher test accuracy. The first step toward resource allocation across different learning rounds is to evaluate the impact of resources on the overall learning accuracy and convergence. We analyze the convergence behavior of FL, specifically, the optimality gap of the loss function in each communication round is presented to depict the relationship between communication accuracy and learning performance. Accordingly, a corresponding performance-oriented design approach is proposed that aims to directly minimize the optimality gap of the learning phase. The performance-oriented design approach is shown as a *later-is-better* principle, which reveals the later rounds in the FL procedure are more sensitive to the aggregation error, hence more communication resources are required over time. The main contributions are summarized as follows.

- We analyze the optimality gap of the loss function over different communication rounds, which characterizes the impact of gradient aggregation errors in different communication rounds on the convergence performance of IRS assisted FL. From the obtained optimality gap, it can be observed that within a finite number of communication rounds, the aggregation errors at later rounds contribute more to the optimality gap than those at earlier rounds. Hence, the later rounds are more essential to the learning performance of FL, thus more communication resources need to be allocated.
- In order to enhance the ultimate performance of FL, we directly minimize the optimality gap with instantaneous and average power constraints. We first propose an offline design approach that is sequentially decomposed across the entire FL procedure based on the available lookahead channel state information (CSI), and then we leverage the Lyapunov framework to convert it to an online design problem over each communication round without foreseeing the future. The transceiver design and the IRS phase

shift tuning are decoupled through the block coordinate descent (BCD) method. Furthermore, we propose an element-wise successive refinement algorithm with low complexity to guide the practical implementation of an IRS with discrete phase shifts constraint.

- We conduct extensive simulations to evaluate the performance of the proposed performance-oriented design framework by considering handwritten digit recognition on the MNIST dataset [42] with a convolution neural network (CNN). Simulation results show that the proposed algorithm can achieve higher test accuracy than the conventional isolated MSE minimization approach eventually, although it may lag behind in the beginning. Besides, it is observed that the online system design approach acquires satisfying performance compared to the offline solution which validates the *later-is-better* principle.

The remainder of this paper is organized as follows. In Section II, we describe the FL model and the IRS assisted AirComp framework. In Section III, we analyze the FL performance and accordingly formulate the performance-oriented optimization problem. In Section IV, we harness an efficient BCD approach to alternatively optimize transceiver and IRS phase shifts. In Section V, we present extensive numerical results to evaluate the proposed algorithm. Finally, this paper concludes in Section VI.

Notations: Scalars are denoted by italic letters, vectors and matrices are denoted by bold-face lower-case and uppercase letters, respectively. $\mathbb{R}^{m \times n}$ and $\mathbb{C}^{m \times n}$ denote the space of $m \times n$ real-valued and complex-valued matrices, respectively. For a complex-valued vector \mathbf{x} , $\|\mathbf{x}\|$ represents the Euclidean norm of \mathbf{x} , $\arg(\mathbf{x})$ denotes the phase of \mathbf{x} , and $\text{diag}(\mathbf{x})$ denotes a diagonal matrix whose main diagonal elements are extracted from vector \mathbf{x} . For a square matrix \mathbf{S} , $\text{tr}(\mathbf{S})$ and \mathbf{S}^{-1} denote its trace and inverse, respectively, while $\mathbf{S} \succeq \mathbf{0}$ means that \mathbf{S} is positive semi-definite, where $\mathbf{0}$ is a zero matrix of proper size. For any general matrix \mathbf{A} , \mathbf{A}^H , $\text{rank}(\mathbf{A})$, and $\mathbf{A}_{i,j}$ denote its conjugate transpose, rank, and (i, j) th entry, respectively. \mathbf{I}_M denotes a identity matrix of size $M \times M$. j denotes the imaginary unit, i.e., $j^2 = -1$. $\mathbb{E}[\cdot]$ denotes the statistical expectation. $|\cdot|$ denotes the cardinality of a given set. $\mathcal{O}(\cdot)$ is the big-O computational complexity notation.

II. SYSTEM MODEL

As depicted in Fig. 1, an IRS assisted FL system under consideration was comprised of K edge devices, an IRS, and a base station (BS) serving as an edge server. Devices and the IRS are coordinated by the BS to realize the collaborative model training through periodical communication and computation. The details of the FL procedure and the IRS assisted over-the-air aggregation are introduced as follows.

A. Federated Learning Procedure

The goal of the FL system is to collectively acquire the desired parameter $\mathbf{w}^* \in \mathbb{R}^d$ that minimized the global loss function with respect to the entire dataset. Instead of uploading all the raw data to the server, each device processes its local

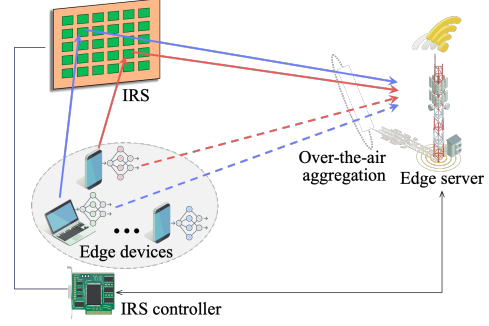


Fig. 1. An IRS assisted AirComp based FL system.

data in parallel and uploads its local parameters or gradients to the server. We adopt the gradient sharing strategy in the FL procedure: the edge devices compute their local gradients and upload them to the edge server, and then the edge server broadcast the aggregated gradient to the edge devices for synchronously local models update.

Specifically, we assume that each edge device holds a subset of training data with $|\mathcal{D}_k|$ samples that are sampled i.i.d. from a source distribution $\mathcal{D} = \bigcup_{k \in \mathcal{K}} \mathcal{D}_k$, which is denoted as $\mathcal{D}_k = \{\mathbf{u}_1, \mathbf{u}_2, \dots, \mathbf{u}_{|\mathcal{D}_k|}\}$. Notation \mathbf{u}_i represents a data sample, which can be represented as a set of feature vectors and its label in supervised learning. The regularized local loss function of the k -th device is given by

$$F_k(\mathbf{w}) = \frac{1}{|\mathcal{D}_k|} \sum_{\mathbf{u}_i \in \mathcal{D}_k} f(\mathbf{w}; \mathbf{u}_i) + \lambda' R(\mathbf{w}), \quad (1)$$

in which $R(\mathbf{w})$ is a strongly convex regularization function, which is scaled by a hyperparameter $\lambda' \geq 0$. The global loss function evaluated at model parameter \mathbf{w} is

$$F(\mathbf{w}) = \frac{1}{D_{\text{tot}}} \sum_{k=1}^K |\mathcal{D}_k| F_k(\mathbf{w}), \quad (2)$$

where $D_{\text{tot}} = \sum_k |\mathcal{D}_k|$. This amounts to the regularized empirical average of the sample-wise loss functions on the global data set \mathcal{D} . The FL procedure aims to obtain the optimal \mathbf{w}^* that minimize the global loss function:

$$\mathbf{w}^* = \arg \min F(\mathbf{w}). \quad (3)$$

To perform cooperative training among edge devices, the edge devices compute their local gradients by minimizing $F_k(\mathbf{w})$ in parallel, and the BS aggregates the global gradient based on gathered local gradients. Specifically, at t -th time slot, with the model parameter before updating denoted by $\mathbf{w}^{(t)}$, each device k computes a gradient vector $\mathbf{g}_k^{(t)}$ based on a randomly sampled mini-batch $\hat{\mathcal{D}}_k$ from the local dataset.

$$\mathbf{g}_k^{(t)} = \nabla F_k(\mathbf{w}^{(t)}) = \frac{1}{|\hat{\mathcal{D}}_k|} \sum_{\mathbf{u}, v \in \hat{\mathcal{D}}_k} \nabla f(\mathbf{w}; \mathbf{u}, v) + \lambda \nabla R(\mathbf{w}^{(t)}). \quad (4)$$

In this paper, we assuming that all the mini-batch size are equal among devices. Hence, the aggregated global gradient at BS is

$$\mathbf{g}^{(t)} = \frac{1}{K} \sum_{k=1}^K \mathbf{g}_k^{(t)}. \quad (5)$$

Then the BS broadcast the global gradient to edge devices for synchronously local model updating. We assume that downlink communication is ideal, hence

$$\mathbf{w}^{(t+1)} = \mathbf{w}^{(t)} - \alpha^{(t)} \cdot \bar{\mathbf{g}}^{(t)}, \quad (6)$$

in which α^t denotes the learning rate in the communication round t .

B. Over-the-air Aggregation

We adopt the AirComp technique to perform the communication-efficient gradient aggregation, and an IRS is deployed to assist the signal transmission from devices to the BS. Edge devices directly transmit the gradient in each time slot¹, without the partition and remapping process as [27], [38]. The system under considering is consisting of K single antenna devices, a BS with M antennas serving as the edge server, and an IRS equipped with N passive elements. The baseband equivalent channels in t -th time slot from the IRS to BS, from the user k to IRS, and from the user k to BS are denoted by $\mathbf{G}^{(t)} \in \mathbb{C}^{M \times N}$, $\mathbf{h}_{r,k}^{(t)} \in \mathbb{C}^{N \times 1}$ and $\mathbf{h}_{d,k}^{(t)} \in \mathbb{C}^{M \times 1}$, respectively. Due to the severe path loss, the power of the signals that are reflected by the IRS two or more times is assumed to be negligible [43]. With the assistance of IRS, the signal received at the BS is given by

$$\mathbf{y}^{(t)} = \sum_{k \in \mathcal{K}} \left(\mathbf{h}_{d,k}^{(t)} + \mathbf{G}^{(t)} \boldsymbol{\Theta}^{(t)} \mathbf{h}_{r,k}^{(t)} \right) b_k^{(t)} \mathbf{g}_k^{(t)} + \mathbf{z}^{(t)}, \quad (7)$$

where $b_k^{(t)} \in \mathbb{C}$ is the transmit factor of device k that controlling the power consumption in t -th slot, and $\mathbf{z}^{(t)} \in \mathbb{C}^d$ denotes the additional white Gaussian noise at the receiver. Besides, $\boldsymbol{\Theta}^{(t)} = \text{diag}(\beta_1^{(t)} e^{j\theta_1^{(t)}}, \dots, \beta_N^{(t)} e^{j\theta_N^{(t)}})$ denotes the diagonal phase shift matrix of the IRS, where $\theta_n^{(t)} \in [0, 2\pi)$, $\beta_n^{(t)} \in [0, 1]$, $\forall n \in \mathcal{N}, \forall t \in \mathcal{T}$ denote the phase shift and the amplitude reflection coefficient on the incident signal of element n . As each element on the IRS is designed to boost the received signals, we assume $\beta_n^{(t)} = 1, \forall n \in \mathcal{N}, \forall t \in \mathcal{T}$ without loss of generality [43], [44]. With applying receive beamformer, the obtained global gradient can be presented as

$$\begin{aligned} \hat{\mathbf{g}}^{(t)} &= \frac{1}{K} \mathbf{m}^{(t)H} \left(\sum_{k \in \mathcal{K}} \tilde{\mathbf{h}}_k^{(t)} b_k^{(t)} \mathbf{g}_k^{(t)} + \mathbf{z}^{(t)} \right) \\ &= \underbrace{\frac{1}{K} \sum_{k \in \mathcal{K}} \mathbf{g}_k^{(t)}}_{\text{desired gradient: } \bar{\mathbf{g}}^{(t)}} \\ &\quad + \underbrace{\frac{1}{K} \sum_{k \in \mathcal{K}} \left(\mathbf{m}^{(t)H} \tilde{\mathbf{h}}_k^{(t)} b_k^{(t)} - 1 \right) \mathbf{g}_k^{(t)} + \frac{\mathbf{m}^{(t)H} \mathbf{z}^{(t)}}{K}}_{\text{aggregation error: } \boldsymbol{\varepsilon}^{(t)}}, \quad (8) \end{aligned}$$

where $\tilde{\mathbf{h}}_k^{(t)} = \mathbf{h}_{d,k}^{(t)} + \mathbf{G}^{(t)} \boldsymbol{\Theta}^{(t)} \mathbf{h}_{r,k}^{(t)}$ denotes the superimposed channel from devices to the BS, and $\boldsymbol{\varepsilon}^{(t)}$ is the aggregation

error caused by the uplink transmission via AirComp. Hence, the local model updating at the devices becomes

$$\mathbf{w}^{(t+1)} = \mathbf{w}^{(t)} - \alpha_t \cdot \hat{\mathbf{g}}^{(t)} = \mathbf{w}^{(t)} - \alpha_t \cdot \left(\bar{\mathbf{g}}^{(t)} + \boldsymbol{\varepsilon}^{(t)} \right). \quad (9)$$

Notice that the aggregated gradient at the edge server in (8) is biased due to perturbation caused by the channel fading and noise. In the next section, we will elaborate on the convergence analysis of the AirComp based FL with perturbed gradients.

III. CONVERGENCE ANALYSIS AND PROBLEM FORMULATION

In this section, we analyze the convergence behavior of FL with the IRS assisted over-the-air gradient aggregation. First, we introduce several assumptions on the loss function $F(\mathbf{w})$ and the stochastic gradient, which are commonly made in the existing literature to facilitate the convergence analysis. Then, the optimality gap is presented to characterize the learning efficiency between two arbitrary communication rounds. The obtained optimality gap sheds light on how the imperfect gradient updates affect the convergence of FL. Therefore, a corresponding performance-oriented design problem is formulated by directly minimizing the optimality gap.

A. Convergence Analysis

In this subsection, we present several assumptions which are fairly standard and have been widely used in the convergence analysis of FL, see e.g., [45]–[47].

Assumption 1 (Smoothness). The global loss function $F(\mathbf{w})$ is smooth at any point $\mathbf{w} \in \mathbb{R}^d$ with constant $L > 0$, that is, it is continuously differentiable and the gradient $\nabla F(\mathbf{w})$ is Lipschitz continuous with constant L , i.e.,

$$\|\nabla F(\mathbf{w}) - \nabla F(\mathbf{w}')\| \leq L \|\mathbf{w} - \mathbf{w}'\|, \forall \mathbf{w}, \mathbf{w}' \in \mathbb{R}^d. \quad (10)$$

Assumption 2 (Polyak-Łojasiewicz (PL) condition [48]). The global loss function $F(\mathbf{w})$ satisfies the PL condition, i.e., for constant $\mu > 0$

$$\|\nabla F(\mathbf{w}^{(t)})\|^2 \geq 2\mu(F(\mathbf{w}^{(t)}) - F(\mathbf{w}^*)). \quad (11)$$

Note that the PL condition is a relaxation of the strong convexity, while it is still a sufficient condition for gradient descent to achieve a linear convergence rate [48]. The μ -strong convexity is the sufficient but unnecessary condition of the μ -PL condition. Therefore, any result based on the μ -PL assumption also applies to the case where μ -strong convexity is assumed [46]. It is noteworthy that while many popular convex optimization problems such as logistic regression and least-squares are often not strongly convex, but satisfy μ -PL condition [48]. Hence, we choose the PL condition instead of the strong convexity.

Assumption 3 (Unbiased estimation). The stochastic gradient evaluated on a mini-batch $\hat{\mathcal{D}}_k \subset \mathcal{D}$ and at any point \mathbf{w} is an unbiased estimator of the partial full gradient, i.e. $\mathbb{E}[\mathbf{g}_k^{(t)}] = \nabla F(\mathbf{w}^{(t)})$.

¹Note that the normalization process to the local gradients is not taken. The normalization procedure is consuming and inapplicable wherein the devices need to calculate the statistics information of the local gradient and even exchange them with each other. These operations are not applicable in our long-term system optimization approach since this information is unpredictable.

Assumption 4 (Bounded variance [46]). The variance of stochastic gradients evaluated on a mini-batch of size B from \mathcal{D} is bounded as

$$\mathbb{E} \left[\|\mathbf{g}_k^{(t)} - \nabla F(\mathbf{w}^{(t)})\|^2 \right] \leq C_1 \|\nabla F(\mathbf{w}^{(t)})\|^2 + \frac{\sigma^2}{B} \quad (12)$$

where C_1 and σ are non-negative constants. Note that the bounded variance assumption (see [46]) is a stronger form of the above with $C_1 = 0$. For ease of representation, we set $C_1 = 0$ as in [46].

Assumption 5 (Bounded sample-wise gradient [49]). At any iteration t , for any training sample (\mathbf{u}, v) , the gradient is upper bounded by a given constant γ_1 , i.e.,

$$\|\nabla f(\mathbf{w}^{(t)}; \mathbf{u}, v)\|^2 \leq \gamma_1. \quad (13)$$

As shown in the following theorem, we elaborate the convergence analysis of FL with perturbed gradients based on the above assumptions.

Theorem 1 (Optimality Gap). Suppose that an FL procedure satisfies Assumptions 1-5, and the learning rate $\alpha^{(t)} \equiv \alpha$ with $\alpha \leq \frac{1}{\mu}$ and $\alpha \leq \frac{1}{L}$, for $\forall T_2 > T_1$, the optimality gap at the end of T_2 -th round compared to the one of T_1 -th will be bounded as (please see it at the top of next page)

Proof. See Appendix A. ■

From Theorem 1, we can observe that the bias term $a_1^{(t)}$ and the MSE term $a_2^{(t)}$ at the later communication rounds contribute more to the optimality gap than that of the initial rounds. Thus, the later rounds are more sensitive to the aggregation error, and more communication resources are required. In the next subsection, we formulate the performance-oriented problem based on the obtained optimality gap.

B. Problem Formulation

1) *Offline Design With ρ -rounds lookahead CSI:* As we focus on the ultimate performance of FL, the goal is to directly minimize the optimality gap in the final round with the maximum power constraint and long-term energy budget constraint of each device. Although (14) can be easily transformed into the case by setting $T_2 = T$, and $T_1 = 0$. However, one critical issue impedes such long-term system optimization, which requires complete offline CSI over the entire FL period (i.e., all the T learning rounds) that is impractical. Hence, we formulate the corresponding performance-oriented optimization problem with ρ -rounds lookahead CSI (i.e., the CSI in the next ρ learning rounds is assumed to be known). Specifically, we divide the entire FL period into $R \geq 1$ periods, each comprising of $\rho \geq 1$ learning rounds such that $T = R\rho$. We assume that all the wireless channels are quasi-static flat-fading and thereby remain constant within each period, or the CSI of each learning round in one period can be precisely predicted via deep learning or other techniques [50]. Note that ρ can be flexibly chosen when facing different channel conditions. According to (14), the optimality gap at the end

of r -th period compared to the one of period $r-1$ is bounded as

$$\begin{aligned} & \mathbb{E} \left[F(\mathbf{w}^{(r\rho+1)}) \right] - F(\mathbf{w}^*) \\ & \leq \underbrace{(1-\mu\alpha)^\rho \left(\mathbb{E} \left[F(\mathbf{w}^{((r-1)\rho+1)}) \right] - F(\mathbf{w}^*) \right)}_{\text{Optimality gap in the end of period } r-1} \\ & \quad + \underbrace{\sum_{t=(r-1)\rho+1}^{r\rho} \gamma_1 \omega_1^{(t)} a_1^{(t)} \gamma_1 + \sum_{t=(r-1)\rho+1}^{r\rho} \omega_2^{(t)} \left(\gamma_2 a_2^{(t)} + \frac{\sigma_z^2 \|\mathbf{m}^{(t)}\|^2}{K^2} \right)}_{g^{(r)}(\{b_k^{(t)}\}, \{\Theta^{(t)}\}, \{\mathbf{m}^{(t)}\})}. \end{aligned} \quad (15)$$

Hence, the ultimate gap at the T -th round (i.e., the end of the R -th period) is bounded as

$$\begin{aligned} & \mathbb{E} \left[F(\mathbf{w}^{(T+1)}) \right] - F(\mathbf{w}^*) \\ & \leq (1-\mu\alpha)^T \left(\mathbb{E} \left[F(\mathbf{w}^{(1)}) \right] - F(\mathbf{w}^*) \right) \\ & \quad + \sum_{r=1}^R (1-\mu\alpha)^{(R-r)\rho} g^{(r)}(\{b_k^{(t)}\}, \{\Theta^{(t)}\}, \{\mathbf{m}^{(t)}\}). \end{aligned} \quad (16)$$

We consider that each edge device is subject to a maximum power constraint P_k^{\max} for each communication round

$$\frac{1}{d} \mathbb{E} \left(\left\| \sqrt{b_k^{(t)}} \mathbf{g}_k^{(t)} \right\|^2 \right) \leq P_k^{\max}, \forall k \in \mathcal{K}, \forall t \in \mathcal{T}, \quad (17)$$

where d is the size of the gradient vector $\mathbf{g}_k^{(t)}$. Besides, in order to reveal the communication resources rationing between different communication rounds, we add another average power constraint of the r -th round which equvalently substitutes the long-term energy budget constraint:

$$\sum_{t=(r-1)\rho+1}^{r\rho} \frac{1}{d} \mathbb{E} \left(\left\| \sqrt{b_k^{(t)}} \mathbf{g}_k^{(t)} \right\|^2 \right) \leq \rho P_k^{\text{avg}}, \forall k \in \mathcal{K}, \forall r \in [1, R]. \quad (18)$$

Due to Assumption 4 and Assumption 5, $\mathbb{E} \left[\|\bar{\mathbf{g}}_k^{(t)}\|^2 \right] \triangleq \tilde{\gamma} \leq \gamma_1 + \frac{\sigma^2}{B}$. Hence, (17) and (18) can be converted into $\tilde{\gamma} |b_k^{(t)}|^2 \leq d \hat{P}_k^{\max}$ and $\sum_{t=(r-1)\rho+1}^{r\rho} \tilde{\gamma} |b_k^{(t)}|^2 \leq \rho d P_k^{\text{avg}}$, respectively. With discarding the constant term in (16), i.e., the initial optimality gap, the corresponding optimization problem can be presented as

$$(P1) : \min_{\substack{\{b_k^{(t)}\}, \\ \{\Theta^{(t)}\}, \{\mathbf{m}^{(t)}\}}} \sum_{r=1}^R (1-\mu\alpha)^{(R-r)\rho} g^{(r)}(\{b_k^{(t)}\}, \{\Theta^{(t)}\}, \{\mathbf{m}^{(t)}\}) \quad (19a)$$

$$\text{s.t.} \quad \tilde{\gamma} |b_k^{(t)}|^2 \leq d P_k^{\max}, \forall k \in \mathcal{K}, \forall t \in \mathcal{T}, \quad (19b)$$

$$\sum_{t=(r-1)\rho+1}^{r\rho} \tilde{\gamma} |b_k^{(t)}|^2 \leq \rho d P_k^{\text{avg}}, \forall k \in \mathcal{K}, \forall r \in [1, R], \quad (19c)$$

$$0 \leq \theta_n^{(t)} \leq 2\pi, \forall n \in \{1, \dots, N\}, \forall t \in \mathcal{T}. \quad (19d)$$

$$\begin{aligned}
& \mathbb{E} \left[F \left(\mathbf{w}^{(T_2+1)} \right) \right] - F(\mathbf{w}^*) \\
& \leq \underbrace{(1 - \mu\alpha)^{(T_2-T_1)} \left(\mathbb{E} \left[F \left(\mathbf{w}^{(T_1+1)} \right) \right] - F(\mathbf{w}^*) \right)}_{\text{Gap of } T_1\text{-th round}} + \underbrace{\sum_{t=T_1+1}^{T_2} (1 - \mu\alpha)^{T_2-t} \frac{(\alpha - L\alpha^2)}{2}}_{\omega_1^{(t)}} \underbrace{\left| \frac{1}{K} (\mathbf{m}^{(t)})^H \sum_{k \in \mathcal{K}} \tilde{\mathbf{h}}_k^{(t)} b_k^{(t)} - 1 \right|^2}_{\text{bias: } a_1^{(t)}} \gamma_1 \\
& \quad + \underbrace{\sum_{t=T_1+1}^{T_2} (1 - \mu\alpha)^{T_2-t} \frac{L\alpha^2}{2}}_{\omega_2^{(t)}} \underbrace{\left\{ \frac{1}{K^2} \sum_{k \in \mathcal{K}} \left| (\mathbf{m}^{(t)})^H \tilde{\mathbf{h}}_k^{(t)} b_k^{(t)} - 1 \right|^2 \right\}}_{\text{MSE: } a_2^{(t)}} \underbrace{\left(\gamma + \frac{\sigma^2}{BK^2} \right)}_{\gamma_2} + \frac{\sigma_z^2 \|\mathbf{m}^{(t)}\|^2}{K^2} \Bigg\}. \tag{14}
\end{aligned}$$

2) *Online Design via Lyapunov Technique:* The previous formulated problem (P1) needs ρ -rounds lookahead CSI. But when facing a fast-varying channel, the CSI may vary within a period, and the channel prediction techniques may induce additional errors. We utilize the Lyapunov optimization framework to construct a virtual energy deficit queue $e_k(t)$ for each device k to guide the power allocation over sequential communication rounds, thus (P1) is transferred to an online optimization problem within different isolated time slots without foreseeing the future.

The virtual energy queue of device k starts with $e_k(t) \geq 0, \forall k$, and is updated at the end of each round t as

$$e_k(t+1) = \max\{\tilde{\gamma}|b_k^{(t)}|^2/d - P_k^{\text{avg}}, 0\} + e_k(t). \tag{20}$$

Hence, $e_k(t)$ indicates the deviation of the current energy consumption of device k from its long-term energy constraint ρP_k^{avg} . Let $\mathbf{e}(t) = \{e_1(t), e_2(t), \dots, e_K(t)\}$ collect the energy deficit queues for all devices. The constructed optimization problem is shown as a weighted sum of the per-round optimality gap and the energy consumption at the devices.

$$\begin{aligned}
\text{(P2)} : \quad & \min_{\{b_k^{(t)}\}, \Theta^{(t)}, \mathbf{m}^{(t)}} V_r (1 - \mu\alpha)^{(R-r)\rho} \left(\gamma_1 \omega_1^{(t)} a_1^{(t)} \right. \\
& \quad \left. + \omega_2^{(t)} \left(\gamma_2 a_2^{(t)} + \frac{\sigma_z^2 \|\mathbf{m}^{(t)}\|^2}{K^2} \right) \right) + \sum_{k \in \mathcal{K}} e_k(t) \frac{\tilde{\gamma}|b_k^{(t)}|^2}{d} \\
& \tag{21a}
\end{aligned}$$

$$\text{s.t. } \tilde{\gamma}|b_k^{(t)}|^2 \leq d P_k^{\text{max}}, \forall k \in \mathcal{K}, \forall t \in \mathcal{T}, \tag{21b}$$

$$0 \leq \theta_n^{(t)} \leq 2\pi, \forall n \in \{1, \dots, N\}, \forall t \in \mathcal{T}. \tag{21c}$$

Where parameter $V_r \geq 0$ is used to adjust the emphasis on the objective function (i.e., optimality gap minimization) in different communication rounds. Notice that if $e_k(t)$ increases in slot t , then minimizing energy consumption is more important in slot $t+1$. Intuitively, when the energy queue is stable, the constraint in (19c) is satisfied. Although problems (P2) and (P1) are not equal due to different objective functions and constraints, the results of (P2) are within a bounded deviation from the optimal results of (P1).

Theorem 2. (P2) achieves a performance-backlog tradeoff of $[\mathcal{O}(1/V), \mathcal{O}(\sqrt{V})]$ with compared to (P1). We use G^* to represent the obtained optimality gap via the optimal offline solution of (P1), and superscript G^\dagger to represent obtained the optimality gap via the optimal offline solution of (P2).

Specifically, the FL performance is $\mathcal{O}(1/V)$ -optimal, which is bounded by

$$\sum_{t=1}^T G_t^\dagger \leq \sum_{t=1}^T G_t^* + \sum_{r=1}^{R-1} \frac{C_r}{V_r}, \tag{22}$$

where $C_r = \rho C_e + \sum_{t=r\rho+1}^{(r+1)\rho} \sum_{k \in \mathcal{K}} E_{\text{max}}((t-1)E_{\text{max}} + e_k(r\rho+1))$, and $E_{\text{max}} = \max_{k,t}(\tilde{\gamma}|b_k^{(t)}|^2/d - P_k^{\text{avg}})$. Besides, the energy consumption is $\mathcal{O}(\sqrt{V})$ -bounded as

$$\begin{aligned}
\sum_{t=1}^T \left(\tilde{\gamma}|b_k^{(t)}|^2/d - P_k^{\text{avg}} \right) & \leq \sum_{r=1}^{R-1} \left(\sqrt{2 \left(C_r + V_r \sum_{t=r\rho+1}^{(r+1)\rho} U_t^* \right)} \right. \\
& \quad \left. - e_k(r\rho+1) \right) \tag{23}
\end{aligned}$$

Proof. See Appendix B. ■

IV. PROPOSED ALGORITHMS FOR OFFLINE AND ONLINE DESIGN

In the previous section, we present an offline optimization problem based on the available lookahead CSI and an online optimization problem via the Lyapunov technique. It can be observed that (P1) can be divided into R subproblems in each period since the constraints and the objective functions are irrelevant across different periods, and (P2) is an online design within each communication round. Note that variables are highly coupled in the objective function, while all the constraints corresponding to each variable are all convex and uncoupled with others in both (P1) and (P2). This thus motivates us to apply the block coordinate descent method to solve them efficiently by properly partitioning the optimization variables into different blocks. We alternately optimize the three blocks of optimization variables as follows. These optimization approaches are similarly in (P1) and (P2), thus the two algorithms are jointly introduced as follows.

A. Power Allocation

With given $\{\Theta^{(t)}\}$ and $\{\mathbf{m}^{(t)}\}$, $\{b_k^{(t)}\}$ need to be precisely rationed in different communication rounds to minimize the ultimate optimality gap. Recall (P1) and (P2), we can obtain the following remark.

Remark 1. In order to minimize the objective function of (P1) and (P2), each device k in t -th time slot always adjusts the phase of its transmit factor $b_k^{(t)}$ for phase compensation

respects to the equivalent fading channel $\bar{h}_k^{(t)} = (\mathbf{m}^{(t)})^H \tilde{\mathbf{h}}_k^{(t)}$, i.e., $\arg[b_k^{(t)}] = \arg[(\bar{h}_k^{(t)})^{-1}]$.

In that case, only the magnitudes of $\{b_k^{(t)}\}$ have effect on the value of the objective function. Let $\bar{b}_k^{(t)}$ denotes the magnitude of b_k , i.e., $\bar{b}_k^{(t)} = |b_k^{(t)}|, \forall k \in \mathcal{K}$. The power allocation problem can be divided into R sub-problems in (P1) since the constraints and the objective function are irrelevant among different periods. By fixing $\arg[b_k^{(t)}] = \arg[(\bar{h}_k^{(t)})^{-1}]$, the power allocation problem of (P1) over one dedicated period can be expressed in the real form as

$$(P1.1) : \min_{\{\bar{b}_k^{(t)}\}} \sum_{t=(r-1)\rho+1}^{r\rho} \gamma_1 \omega_1^{(t)} \left(\frac{1}{K} \sum_{k \in \mathcal{K}} |\bar{h}_k^{(t)}| \bar{b}_k^{(t)} - 1 \right)^2 + \sum_{t=(r-1)\rho}^{r\rho} \frac{\gamma_2 \omega_2^{(t)}}{K^2} \sum_{k \in \mathcal{K}} \left(|\bar{h}_k^{(t)}| \bar{b}_k^{(t)} - 1 \right)^2 \quad (24a)$$

$$\text{s.t. } \tilde{\gamma}(\bar{b}_k^{(t)})^2 \leq dP_k^{\max}, \forall t \in [(r-1)\rho+1, r\rho], \forall k \in \mathcal{K}, \quad (24b)$$

$$\sum_{t=(r-1)\rho+1}^{r\rho} \tilde{\gamma}(\bar{b}_k^{(t)})^2 \leq \rho dP_k^{\max}, \forall t \in [(r-1)\rho+1, r\rho]. \quad (24c)$$

(P1.1) is a convex quadratic optimization problem that can be optimally solved by the standard convex optimization techniques such as the interior point method or alternating direction method of multipliers (ADMM). In the subsequent, we resort to the Lagrange duality method to derive the structured optimal solution for problem (P1.1) to gain engineering insights. Let $\{\lambda_k^*\}$ denote the optimal dual variable associated with the k -th constraint in (24c). Then, the optimal solution of $\bar{b}_k^{(t)}$ can be obtained through the first-order optimality condition:

$$(\bar{b}_k^{(t)})^* = \min \left\{ \frac{\gamma_1 \omega_1^{(t)} (K - \sum_{i \neq k} |\bar{h}_i^{(t)}| \bar{b}_i^{(t)}) + \gamma_2 \omega_2^{(t)}}{\left(\gamma_1 \omega_1^{(t)} + \gamma_2 \omega_2^{(t)} \right) |\bar{h}_k^{(t)}| + \frac{K^2}{|\bar{h}_k^{(t)}|} \sum_k \lambda_k^*}, \sqrt{dP_k^{\max}/\tilde{\gamma}} \right\}. \quad (25)$$

The optimal dual variable $\{(\lambda_k^*)^*\}$ can be obtained through subgradient based methods as shown in [29].

Considering the special case when the average power budget are not less than the maximum power constraint at all devices, i.e., $P_k^{\text{avg}} \geq P_k^{\max}, \forall k \in \mathcal{K}$. In this case, the average power constraints are not activated, the dual variables are equal to zero (i.e., $\lambda_k^* = 0$). The proposed optimal power allocation strategy degrades into the isolated optimization across different time slots, and exhibits a threshold-based structure: all the devices $k \in \mathcal{K}'$ that satisfy $|\bar{h}_i^{(t)}| \sqrt{dP_k^{\max}/\tilde{\gamma}} - 1 < 0$, should transmit signals with the largest power; otherwise, the devices $k \notin \mathcal{K}'$ that satisfy $|\bar{h}_i^{(t)}| \sqrt{dP_k^{\max}/\tilde{\gamma}} - 1 \geq 0$, should enlarge their transmit power moderately (overcompensate their channel) to minimize the optimality gap caused by the deep faded channel of the devices $k \in \mathcal{K}'$. As for the conventional isolated MSE minimization approach, the devices $k \in \mathcal{K}'$ still transmit with the largest power, while the devices $k \notin \mathcal{K}'$ only compensate their individual channels to minimize the MSE without further

decreasing the optimality gap. While, for the general case that the average power budgets are less than the maximum power constraint at all devices, i.e., $P_k^{\text{avg}} < P_k^{\max}, \forall k \in \mathcal{K}$. In this case, the dual variables in (25) are larger than zero (i.e., $\lambda_k^* > 0$). The power allocation are closed related to the chronological order and the current channel condition due to the additional term $\frac{K^2}{|\bar{h}_k^{(t)}|} \sum_k \lambda_k^*$ in the denominator. It can be observed that a larger power will be allocated to the devices in the later time slots and/or with better channel conditions. While the optimal power control method of the conventional isolated MSE minimization approach still remains the same as the one with $P_k^{\text{avg}} \geq P_k^{\max}, \forall k \in \mathcal{K}$ by substituting the maximum power to P_k^{avg} .

As for (P2), the power control in one dedicated communication round is still a convex optimization problem and the optimal solution is

$$(\bar{b}_k^{(t)})^\dagger = \min \left\{ \frac{\gamma_1 \omega_1^{(t)} (K - \sum_{i \neq k} |\bar{h}_i^{(t)}| \bar{b}_i^{(t)}) + \gamma_2 \omega_2^{(t)}}{(\gamma_1 \omega_1^{(t)} + \gamma_2 \omega_2^{(t)}) |\bar{h}_k^{(t)}| + \frac{K^2}{|\bar{h}_k^{(t)}|} \frac{e_k(t) \tilde{\gamma}}{dV_r(1-\mu\alpha)^{(R-r)\rho}}}, \sqrt{dP_k^{\max}/\tilde{\gamma}} \right\}. \quad (26)$$

Comparing with (25), the term $\frac{e_k(t) \tilde{\gamma}}{dV_r(1-\mu\alpha)^{(R-r)\rho}}$ substitutes the term $\sum_k \lambda_k^*$ in (25). It can be observed that with a larger $e_k(t)$ and/or a smaller V_r , more energy will be allocated in current round.

B. Receiver Design

With the given power allocation and the phase shift of IRS, the optimization problems with respect to the receive beamformers $\{\mathbf{m}^{(t)}\}$ of (P1) and (P2) can be separated among different time slots. Hence, the corresponding subproblem with omitting the time index can be written as

$$(P1.2) : \min_{\mathbf{m}} \gamma_1 \omega_1 \left| \frac{1}{K} \mathbf{m}^H \sum_{k \in \mathcal{K}} \hat{\mathbf{h}}_k b_k - 1 \right|^2 + \gamma_2 \omega_2 \left(\frac{\gamma_2}{K^2} \sum_{k \in \mathcal{K}} \left| \mathbf{m}^H \hat{\mathbf{h}}_k b_k - 1 \right|^2 + \frac{\sigma_z^2 \|\mathbf{m}\|^2}{K^2} \right). \quad (27)$$

Since problem (P1.2) is an unconstrained convex problem, by exploiting the first-order optimality condition, the closed-form solution for \mathbf{m} is given by

$$\mathbf{m}^* = \left(\gamma_1 \omega_1 \sum \tilde{\mathbf{h}}_k b_k + \gamma_2 \omega_2 \sum |b_k|^2 \tilde{\mathbf{h}}_k \tilde{\mathbf{h}}_k^H + \omega_2 \sigma_z^2 \mathbf{I} \right)^{-1} \times \left((K \gamma_1 \omega_1 + \gamma_2 \omega_2) \sum \tilde{\mathbf{h}}_k b_k \right). \quad (28)$$

The optimal receiver given above is shown as a weighted summed structure compared to the conventional minimum mean square error (MMSE) receiver. In particular, the conventional MMSE receiver is $\left(\sum_{k \in \mathcal{K}} |b_k|^2 \tilde{\mathbf{h}}_k \tilde{\mathbf{h}}_k^H + \sigma_z^2 \mathbf{I} \right)^{-1} \tilde{\mathbf{h}}_k b_k$ that is aiming for estimating the individual message of dedicated device k . Besides, the receiver in the AirComp based FL system via the isolated MSE minimization approach is $\left(\sum_{k \in \mathcal{K}} |b_k|^2 \tilde{\mathbf{h}}_k \tilde{\mathbf{h}}_k^H + \sigma_z^2 \mathbf{I} \right)^{-1} \left(\sum_k \tilde{\mathbf{h}}_k b_k \right)$, which can be

similarly obtained by exploiting the first-order optimality condition to the second term in (27). This receiver is targeted at computing the sum of local gradients $\sum_k \mathbf{g}_k, k \in \mathcal{K}$. While the optimal receiver (28) of the proposed performance-oriented approach is shown as a weighted summation structure, with the corresponding weights be the ones of the bias term and the MSE term in the optimality gap in (14).

C. Phase Shift Optimization of the IRS

With the given power allocation and the receiver beamformer, the optimization problem with respect to the phase shift $\{\Theta^{(t)}\}$ of IRS can be separated among different time slots. By multiply by a constant term K^2 , the optimization can be presented as

$$(P1.3) : \min_{\Theta} \gamma_1 \omega_1 \underbrace{\left| \mathbf{m}^H \sum_{k \in \mathcal{K}} \tilde{\mathbf{h}}_k^{(t)} b_k - K \right|^2}_{a'_1} + \gamma_2 \omega_2 \sum_{k \in \mathcal{K}} \underbrace{\left| \mathbf{m}^H \tilde{\mathbf{h}}_k^{(t)} b_k - 1 \right|^2}_{a'_2} \quad (29a)$$

$$\text{s.t. } 0 \leq \theta_n \leq 2\pi, \forall n \in \{1, \dots, N\}. \quad (29b)$$

Since (P1.3) is a non-convex optimization problem due to the per-phase constraints in (29b). We first apply the semidefinite relaxation (SDR) strategy to relax (P1.3) into a semidefinite programming (SDP) problem. To reduce the practical computational complexity, we further propose an element-wise optimization approach to achieve near-optimal performance. Besides, the proposed element-wise optimization approach can be easily extended to the practical scenario with discrete phase shifts constraint.

1) *SDR Approach*: Let $\mathbf{v} = [e^{j\theta_1}, \dots, e^{j\theta_N}]^H$, (P1.3) can be transformed to a convex optimization problem with norm-1 constraint. Furthermore, the matrix lifting technique can be applied to convert it to an SDP problem [43], [51], [52] with rank-1 constraint by lifting the vector into a positive semidefinite (PSD) matrix. Then, we apply the well-known SDR technique to drop the non-convex rank-1 constraint. Hence, an SDP problem is formed which can be solved efficiently in polynomial time by existing convex optimization solvers such as CVX. If the optimal solution to the SDP problem is rank-1, the optimal solution to the original problem can be recovered by applying singular value decomposition (SVD) to \mathbf{V}^* . While, if the optimal solution to the SDP problem is obtained with a higher rank, additional steps such as Gaussian randomization [52] need to be applied to extract a suboptimal solution for the original problem.

2) *Low-complexity Suboptimal Solution*: Although a satisfying solution to (P1.3) can be obtained through the SDR approach, the lifted optimization variable induces more computation complexity. Solving a series of high-dimensional SDP problems increases the computational burden drastically and the additional steps to extract a suboptimal solution are often with intolerable computation consumption, especially when facing an IRS with large-scale elements which are common in practice. Besides, the obtained continuous phase shifts

at reflecting elements are practically difficult to implement due to hardware limitations. Generally, the discrete phase shifts optimization problem is shown as an integer linear program problem that can be optimally solved via the branch-and-bound with the worst-case exponential complexity [53]. Hence, in order to reduce the computational complexity and provided the near-optimal solution for the IRS with discrete phase shifts constraint, we successively refine the phase shift of each element until converges. It is noted that the phase shifts of all elements are fully separable in (P1.3), and only coupled in the objective function. Hence, we can successively optimize the phase shift of each element until converges. Specifically, we alternately optimize each phase shift in an iterative manner by fixing the other $N-1$ phase shifts, until the convergence is achieved. For a given $n \in N$, by fixing the others, the objective function in (P1.3) is linear with respect to $e^{j\theta_n}$, which can be written as

$$\begin{aligned} & \gamma_1 \omega_1 \left(\mathbf{v}^H \underbrace{\boldsymbol{\psi} \boldsymbol{\psi}^H}_{\boldsymbol{\Psi}'} \mathbf{v} + 2\Re\{\mathbf{v}^H \underbrace{\boldsymbol{\psi} \zeta^H}_{\zeta'}\} + |\zeta|^2 \right) \\ & + \gamma_2 \omega_2 \sum_{k \in \mathcal{K}} \left(\mathbf{v}^H \underbrace{\boldsymbol{\phi}_k \boldsymbol{\phi}_k^H}_{\boldsymbol{\Phi}'_k} \mathbf{v} + 2\Re\{\mathbf{v}^H \underbrace{\boldsymbol{\phi}_k \varphi_k^H}_{\varphi'_k}\} + |\varphi_k|^2 \right) \\ & = \gamma_1 \omega_1 \left(\sum_{l \neq n} \sum_{i \neq n} \boldsymbol{\Psi}'(l, i) e^{j(\theta_l - \theta_i)} + 2\Re\{e^{j\theta_n} q_n^{(1)}\} + C' \right) \\ & + \gamma_2 \omega_2 \left(\sum_{k=1}^K \sum_{l \neq n} \sum_{i \neq n} \boldsymbol{\Phi}'_k(l, i) e^{j(\theta_l - \theta_i)} \right. \\ & \quad \left. + 2\Re\{e^{j\theta_n} \sum_{k=1}^K q_{k,n}^{(2)}\} + \sum_{k=1}^K C_k \right). \end{aligned} \quad (30)$$

The constant terms in the above are given by

$$q_n^{(1)} = \sum_{l \neq n} \boldsymbol{\Psi}'(n, l) e^{-j\theta_l} + \zeta'(n) = |q_n^{(1)}| e^{j\nu_n}, \quad (31)$$

$$C' = \boldsymbol{\Psi}'(n, n) + 2\Re\left\{ \sum_{l \neq n} e^{j\theta_l} \zeta'(l) \right\} + |\zeta'|^2, \quad (32)$$

$$\sum_{k=1}^K q_{k,n}^{(2)} = \sum_{k=1}^K \left(\sum_{l \neq n} \boldsymbol{\Phi}'_k(n, l) e^{-j\theta_l} + \varphi'_k(n) \right) = |q_n^{(2)}| e^{j\varsigma_n}, \quad (33)$$

$$C_k = \boldsymbol{\Phi}'_k(n, n) + 2\Re\left\{ \sum_{l \neq n} e^{j\theta_l} \varphi'_k(l) \right\} + |\varphi'_k|^2. \quad (34)$$

Thus we need to minimize the part related to the n -th element, which can be equivalently transformed to the following by leveraging the trigonometric identities:

$$\begin{aligned} & \gamma_1 \omega_1 \Re\{e^{j\theta_n} q_n^{(1)}\} + \gamma_2 \omega_2 \Re\left\{ e^{j\theta_n} \sum_{k=1}^K q_{k,n}^{(2)} \right\} \\ & = \gamma_1 \omega_1 |q_n^{(1)}| \sin(\theta_n + \nu_n + \frac{\pi}{2}) + \gamma_2 \omega_2 |q_n^{(2)}| \sin(\theta_n + \varsigma_n + \frac{\pi}{2}) \\ & = \hat{c}_n \sin(\theta_n + \hat{\theta}_n), \end{aligned} \quad (35)$$

with

$$\hat{\theta}_n = \text{atan2}(\gamma_2\omega_2|q_n^{(2)}|\sin(\zeta_n - \nu_n), \gamma_1\omega_1|q_n^{(1)}| + \gamma_2\omega_2|q_n^{(2)}|\cos(\zeta_n - \nu_n)). \quad (36)$$

When $\gamma_1\omega_1|q_n^{(1)}| + \gamma_2\omega_2|q_n^{(2)}|\cos(\zeta_n - \nu_n) > 0$, $\hat{\theta}_n = \text{atan}\frac{\gamma_2\omega_2|q_n^{(2)}|\sin(\zeta_n - \nu_n)}{\gamma_1\omega_1|q_n^{(1)}| + \gamma_2\omega_2|q_n^{(2)}|\cos(\zeta_n - \nu_n)} \in [-\frac{\pi}{2}, \frac{\pi}{2}]$, otherwise $\hat{\theta}_n = \pi + \text{atan}\frac{\gamma_2\omega_2|q_n^{(2)}|\sin(\zeta_n - \nu_n)}{\gamma_1\omega_1|q_n^{(1)}| + \gamma_2\omega_2|q_n^{(2)}|\cos(\zeta_n - \nu_n)} \in [\frac{\pi}{2}, \frac{3\pi}{2}]$.

Hence, the optimal phase shift of the n -th element is

$$\theta_n^* = \frac{3}{2}\pi - \hat{\theta}_n. \quad (37)$$

For ease of practical implementation, we consider that the phase shift at each element of the IRS can take only a finite number of discrete values. Let δ denotes the number of bits used to indicate the number of phase shift levels. For simplicity, we assume that such discrete phase-shift values are obtained by uniformly quantizing the interval $[0, 2\pi)$. Thus, the set of discrete phase shift values at each element is given by $\mathcal{S} = \{0, \Delta\theta, \dots, (2^\delta - 1)\Delta\theta\}$ with $\Delta\theta = 2\pi/2^\delta$. Hence, the optimal configuration with finite quantization bit is $\bar{\theta}_n^* = \arg \min_{\theta \in \mathcal{S}} |\theta - \theta_n^*|$. With successively setting the phase shifts of all elements based on the above, the objective value will be non-increasing over the iterations until converges.

Overall Algorithm and Computational Complexity Analysis: Based on the provided solutions to the above three subproblems, an efficient BCD algorithm is proposed, where the IRS beamforming vector and transceiver are alternately optimized until convergence is achieved. Note that the objective value of problem (P1) is bounded and non-decreasing by alternately optimizing $\{\mathbf{m}^{(t)}\}$, $\{b_k^{(t)}\}$ and $\{\Theta^{(t)}\}$. Besides, the variables are only coupled in the objective function in (P1). Thus, the proposed BCD algorithm is guaranteed to converge to a stationary point of (P1). The proposed BCD algorithm is guaranteed to converge to a local minimum point. The mainly computational complexity of the proposed BCD algorithm lies in solving the sub-problems (P1.1), (P1.2), and (P1.3). Specifically, the corresponding computational complexity is given by $\mathcal{O}((\rho K)^{3.5})$, $\mathcal{O}(\rho)$ and $\mathcal{O}(\rho NI'_{iter})$, respectively. Where I'_{iter} number of iterations required in the element-wise optimization of discrete phase shifts. Therefore, the total complexity of the BCD algorithm is $\mathcal{O}(((\rho K)^{3.5} + \rho(NI'_{iter} + 1))I_{iter})$, where I_{iter} denotes the number of iterations required to reach convergence of the objective function.

(P2) is an online system design problem that is operated in each communication round. From Theorem 2, we can obtain (P2) is only a bounded substitution for (P1). V_r is utilized to control the trade-off between the sizes of the queue backlogs and the objective function value. It is noted that an increasing V_r will strengthen the emphasis on the optimality gap minimization rather than power minimization in the later rounds, therefore the ultimate performance can be promoted. Besides, if the $e_k(r\rho + 1)$ is initialized to 0 as commonly set in the existing literature [40], (P2) is reduced to an optimality gap minimization problem in the initial round without virtual energy constraint. In that case, the obtained power allocation

in the current communication round is most like to exceed the average power constraint, which obviously deviates from the optimal allocation. The total complexity of the BCD algorithm for (P2) is $\mathcal{O}((\rho K + \rho(NI'_{iter} + 1))I_{iter})$.

V. SIMULATION RESULTS

In this section, we conduct extensive simulation results to validate the performance of the proposed performance-oriented design approach for IRS assisted FL. Simulations are operated for handwritten recognition task via CNN on the MNIST dataset. First, the convergence behavior of the proposed optimality gap minimization algorithm was presented. Then, we analyze the test accuracy under different parameters, e.g., ρ that determines the available CSI which is highly related to the power allocation in different time slots, and the number of IRS elements N which determines the capability to configure the wireless channel. Finally, we compared the performance of offline and online design approaches.

A. Simulation Setup

We consider a three-dimensional coordinate system, where the BS and the IRS are respectively located at $(0, 0, 30)$ and $(0, 50, 20)$ meters. In addition, the edge devices are randomly distributed in the circle region centered at $(50, 40, 0)$ with the radius equals to 20 meters. The wireless channels from the devices to the BS over different communication rounds follow i.i.d. Rayleigh fading, and the channels from IRS to BS and devices follow Rician fading. The path loss model under consideration is $L(d) = T_0(d/d_0)^\alpha$, where $T_0 = -30$ dB is the path loss at reference distance $d_0 = 1$ meter, d is the signal distance, and α is the path loss exponent. The path loss exponents for the BS-device link, the BS-IRS link, and the IRS-device link are set to 3.5, 2.2, and 2.5, respectively. The other parameters are set as follows: $P_k^{\max} = 10$ dBm and $P_k^{\text{avg}} = 6$ dBm, $\sigma_z^2 = -80$ dBm. Other parameters in the assumptions are set as $\mu = 0.2$, $L = 10$, $\sigma^2 = 1000$, $\gamma_1 = 2000$, respectively [54].

B. Simulations Results

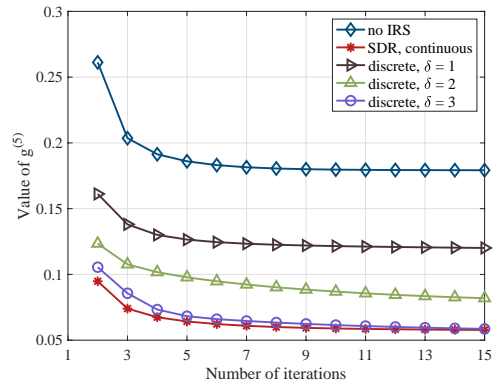


Fig. 2. Convergence behavior of proposed algorithm.

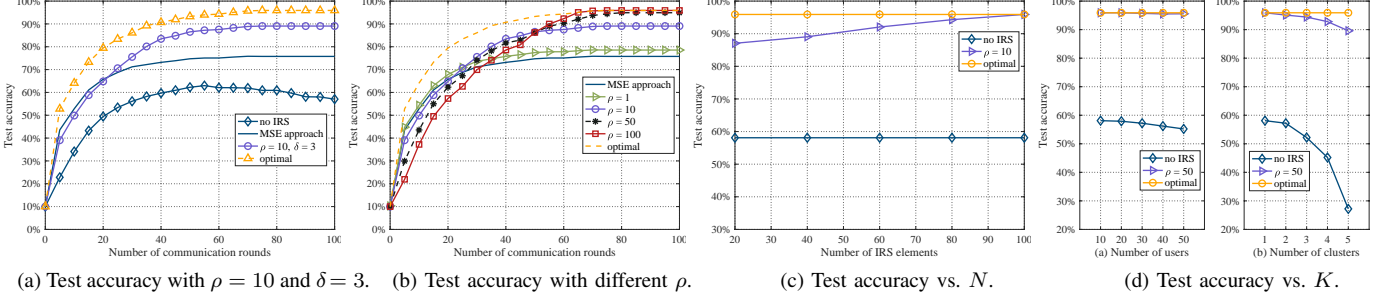


Fig. 3. The performance of offline design approach.

First, the convergence behavior of the proposed optimality gap minimization algorithm is shown in Fig. 2. Since (P1) is optimized within each r -th period, we set $T = 100$, $R = 10$, and $\rho = 10$. The convergence behavior of the proposed optimality gap minimization algorithm conducted on the 5-th period (i.e., 40 to 50 time slots) is presented. The number of devices is fixed to $K = 20$. For the case without IRS, the phase shifts matrix is fixed to $\Theta = \mathbf{0}$. For the case with IRS, the number of the IRS elements is fixed to $N = 40$, and the number of antennas equipped at BS is set to $M = 5$. It is shown that the IRS can significantly diminish the optimality gap even with a finite configuration range such as the quantization bit equals 1. Besides, the performance of IRS with a quantization level of 3 can achieve nearly the same performance as the one with continuous phase shifts.

Then, the IRS-assisted FL was deployed for handwritten recognition on the MNIST dataset. We implement a 3-layer CNN as the classifier model, which consists of an input layer, a final softmax output layer, and a midterm convolution layer with max pooling. The local batch size at each edge device is set to $B = 64$, and the learning rate α_t is fixed to 0.005. Besides, we compare the learning performance with the following two benchmark schemes:

- **Optimal aggregation:** The wireless channels are ideal, thus the server can aggregate precise local gradients for the global model update.
- **Conventional MSE minimization:** Parameters are optimized to minimize the MSE of aggregated gradients in isolation as [27]. The transceiver and the phase shift of IRS are alternatively optimized. Note that the average power constraint degraded to the maximum power constraint in such an isolated optimization approach.

As shown in Fig. 3a, the proposed optimality gap minimization algorithm is observed to outperform the conventional MSE minimization approach. This is due to the fact that the contributions of aggregation errors to the optimality gap are distinct at different communication rounds, which cannot be captured by the conventional MSE minimization design. It is observed in the beginning, the performance of all schemes shows an increasing trend. The proposed algorithm is inferior to the traditional MSE minimization design approach in the initial, but it speeds up and eventually outperforms in the later rounds. Besides, the performance of the FL without the assistance of the IRS deteriorates heavily as the number of communication rounds increases. It is due to the model

aggregation error in the latter rounds deteriorating the learning performance greater than the beginning, thereby increasing the gap between others. Note that the system optimization is operated based on each ρ round lookahead CSI, therefore, the available CSI is closely related to the system performance. Fig. 3b depicts the test accuracy under different ρ . It can be observed that the ultimate performance of the proposed algorithm monotonically increases with ρ since more communication rounds are integrated optimized. Moreover, one can observe that the performance declines in the initial as the ρ goes, but rises and exceeds in the later rounds. These observations are consistent with the convergence analysis in the former sections which further demonstrate the necessity and efficiency of such a performance-oriented design approach.

Then, we investigate the test accuracy versus the number of IRS elements and the number of users. As shown in Fig. 3c, the test accuracy of the proposed algorithm with $\rho = 10$ is monotonically increased with N until converges to the optimal. By comparing Fig. 3c to Fig. 3b, we can observe that a larger scale IRS can diminish the performance deterioration due to the lack of lookahead CSI. Hence, when the CSI is varying or can not be precisely predicted e.g., facing the fast-varying channel, the IRS with more elements can configure a more favorable communication link thus obtaining higher test accuracy in FL. The performance between FL with IRS and the one without IRS is further compared with the varying numbers of users. Specifically, the devices are distributed in one cluster in the setting of Fig. 3d(a), and users are distributed in various clusters in the setting of Fig. 3d(b). The users are randomly distributed in 5 circle regions with the radii equal to 20 meters, the centers are located from (50, 40, 0) to (130, 40, 0) with the coordinates of the first dimension are incremented by 20 in sequence. From Fig. 3d(a), it is observed that the test accuracy decays slightly as the number of devices increases even without the help of IRS. While the one with IRS can still obtain a satisfying test accuracy with tiny performance loss. This result verifies that AirComp is an efficient data aggregation approach for model aggregation in FL. Then redirects to Fig. 3d(b), it can be observed that both the performance of the one with or without IRS decays as the number of clusters increases. This is due to the performance of AirComp is determined by the device with the worst channel. But the FL system can still maintain a satisfying performance with the help of IRS.

Finally, we compare the performance between offline and online design schemes. The total FL procedure contains $T =$

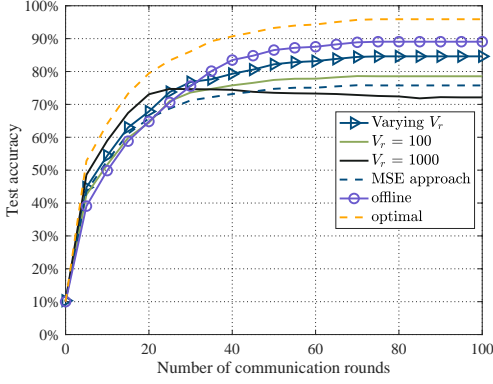


Fig. 4. Test accuracy of online design approach.

100 rounds with $\rho = 10$. For the offline design, we choose an varying V_r sequence with $V_r = 100 * \sqrt{(10r + 1)}$ and two V_r fixed to 100 and 1000, respectively. Besides, $e_k(r\rho + 1), \forall r$ are initialized as $0.2P_k^{\text{avg}}$. Fig. 4 validates that the online design approach with varying V_r can obtain higher test accuracy than the fixed V_r . An increasing V_r leads to larger power allocation in the latter rounds in FL, thus better performance can be obtained. The online design approach with V_r fixed to 1000 obtains the near-optimal performance in the beginning, but results in extreme energy consumption which is destructive to the latter rounds.

VI. CONCLUSION

In this paper, we proposed a performance-oriented design framework for IRS assisted FL system. With elaborately analyzing the convergence behavior of FL, a corresponding optimality gap minimization problem was established. We adopted the BCD method to tackle the highly-intractable problem. Simulation results demonstrated that such a performance-oriented design algorithm can precisely allocate the communication resources to different time slots, hence achieving higher test accuracy and faster convergence behavior in FL than the conventional MSE minimization approach. Besides, the employed IRS can assist AirComp to provide precise model aggregation in FL, especially when the lookahead CSI is limited or devices are vastly distributed. Finally, we validated that the online design approach via the Lyapunov framework can achieve satisfying performance without foreseeing the future. The relationship between communication accuracy and learning performance presented in the paper is rigorously depicted via mathematical proof and simulation verification, which is shown as a *later-is-better* principle that can provide significant guidance for the FL system design.

APPENDIX A: PROOF OF THEOREM 1

According to Assumption 1, we can obtain that

$$\begin{aligned} & F(\mathbf{w}^{(t+1)}) - F(\mathbf{w}^{(t)}) \\ & \leq \langle \nabla F(\mathbf{w}^{(t)}), (\mathbf{w}^{(t+1)} - \mathbf{w}^{(t)}) \rangle + \frac{L}{2} \|\mathbf{w}^{(t+1)} - \mathbf{w}^{(t)}\|^2 \\ & = -\alpha_t \langle \nabla F(\mathbf{w}^{(t)}), (\bar{\mathbf{g}}^{(t)} + \boldsymbol{\varepsilon}^{(t)}) \rangle + \frac{L\alpha_t^2}{2} \|\bar{\mathbf{g}}^{(t)} + \boldsymbol{\varepsilon}^{(t)}\|^2. \end{aligned} \quad (38)$$

With $\alpha_t \leq \frac{1}{L}$, by taking expectation with respect to the stochastic gradient and the aggregation error on both sides of (38), we have

$$\begin{aligned} & \mathbb{E} [F(\mathbf{w}^{(t+1)}) - F(\mathbf{w}^{(t)})] \\ & \leq -\alpha_t \mathbb{E} [\langle \nabla F(\mathbf{w}^{(t)}), (\bar{\mathbf{g}}^{(t)} + \boldsymbol{\varepsilon}^{(t)}) \rangle] + \frac{L\alpha_t^2}{2} \mathbb{E} [\|\bar{\mathbf{g}}^{(t)} + \boldsymbol{\varepsilon}^{(t)}\|^2] \\ & \stackrel{a}{=} -\alpha_t \|\nabla F(\mathbf{w}^{(t)})\|^2 - \alpha_t \langle \nabla F(\mathbf{w}^{(t)}), \mathbb{E}[\boldsymbol{\varepsilon}^{(t)}] \rangle \\ & \quad + \frac{L\alpha_t^2}{2} \mathbb{E} [\|\bar{\mathbf{g}}^{(t)}\|^2] + L\alpha_t^2 \langle \nabla F(\mathbf{w}^{(t)}), \mathbb{E}[\boldsymbol{\varepsilon}^{(t)}] \rangle \\ & \quad + \frac{L\alpha_t^2}{2} \mathbb{E} [\|\boldsymbol{\varepsilon}^{(t)}\|^2] \\ & \stackrel{b}{\leq} -\alpha_t \|\nabla F(\mathbf{w}^{(t)})\|^2 + \frac{L\alpha_t^2}{2} \mathbb{E} [\|\bar{\mathbf{g}}^{(t)}\|^2] + \frac{L\alpha_t^2}{2} \mathbb{E} [\|\boldsymbol{\varepsilon}^{(t)}\|^2] \\ & \quad + \frac{(\alpha_t - L\alpha_t^2)}{2} (\|\nabla F(\mathbf{w}^{(t)})\|^2 + \|\mathbb{E}[\boldsymbol{\varepsilon}^{(t)}]\|^2), \end{aligned} \quad (39)$$

where a is due to Assumption 3, b is due to the Cauchy-Schwarz inequality and the inequality of arithmetic and geometric means: $\pm \mathbf{x}_1^T \mathbf{x}_2 \leq \|\mathbf{x}_1\| \|\mathbf{x}_2\| \leq \frac{\|\mathbf{x}_1\|^2}{2} + \frac{\|\mathbf{x}_2\|^2}{2}$.

Due to Assumption 4 and Assumption 5, we have

$$\begin{aligned} & \mathbb{E}_t [\|\bar{\mathbf{g}}^{(t)} - \nabla F(\mathbf{w}^{(t)})\|^2] \\ & = \frac{1}{K^2} \mathbb{E}_t \left[\left\| \sum_k (\mathbf{g}_k^{(t)} - \nabla F(\mathbf{w}^{(t)})) \right\|^2 \right] \leq \frac{\sigma^2}{BK^2}. \end{aligned} \quad (40)$$

Besides,

$$\begin{aligned} & \mathbb{E}_t [\|\bar{\mathbf{g}}^{(t)} - \nabla F(\mathbf{w}^{(t)})\|^2] \\ & = \mathbb{E}_t [\|\bar{\mathbf{g}}^{(t)}\|^2] - \|\nabla F(\mathbf{w}^{(t)})\|^2 \leq \frac{\sigma^2}{BK^2}. \end{aligned} \quad (41)$$

Hence,

$$\mathbb{E}_t [\|\bar{\mathbf{g}}^{(t)}\|^2] \leq \|\nabla F(\mathbf{w}^{(t)})\|^2 + \frac{\sigma^2}{BK^2} \leq \gamma_1 + \frac{\sigma^2}{BK^2}. \quad (42)$$

According to Assumption 2, and with $\alpha^{(t)} \equiv \alpha, \alpha \leq \frac{1}{\mu}, \alpha \leq \frac{1}{L}$, we have

$$\begin{aligned} & \mathbb{E} [F(\mathbf{w}^{(t+1)})] - F(\mathbf{w}^*) \\ & \leq (1 - \mu\alpha) (\mathbb{E} [F(\mathbf{w}^{(t)})] - F(\mathbf{w}^*)) \\ & \quad + \frac{(\alpha - L\alpha^2)}{2} \mathbb{E} [\|\boldsymbol{\varepsilon}^{(t)}\|^2] + \frac{L\alpha^2}{2} \mathbb{E} [\|\boldsymbol{\varepsilon}^{(t)}\|^2] + \frac{L\alpha^2\sigma^2}{2BK^2}. \end{aligned} \quad (43)$$

Recursively applying (43), finally we obtain that for $\forall T_2 > T_1$,

$$\begin{aligned} & \mathbb{E} [F(\mathbf{w}^{(T_2+1)})] - F(\mathbf{w}^*) \\ & \leq (1 - \mu\alpha)^{(T_2-T_1)} (\mathbb{E} [F(\mathbf{w}^{(T_1+1)})] - F(\mathbf{w}^*)) \\ & \quad + \sum_{t=T_1+1}^{T_2} (1 - \mu\alpha)^{T_2-t} \left\{ \frac{(\alpha - L\alpha^2)}{2} \mathbb{E} [\|\boldsymbol{\varepsilon}^{(t)}\|^2] \right. \\ & \quad \left. + \frac{L\alpha^2}{2} \mathbb{E} [\|\boldsymbol{\varepsilon}^{(t)}\|^2] + \frac{L\alpha^2\sigma^2}{2BK^2} \right\} \end{aligned} \quad (44)$$

Recall (8), we can obtain

$$\left\| \mathbb{E} [\varepsilon^{(t)}] \right\|^2 = \left\| \frac{1}{K} (\mathbf{m}^{(t)})^H \sum_k \tilde{\mathbf{h}}_k^{(t)} b_k^{(t)} - 1 \right\|^2 \|\nabla F(\mathbf{w}^{(t)})\|^2, \quad (45)$$

$$\begin{aligned} & \mathbb{E} \left[\left\| \varepsilon^{(t)} \right\|^2 \right] \\ &= \frac{\sum_k \left| (\mathbf{m}^{(t)})^H \tilde{\mathbf{h}}_k^{(t)} b_k^{(t)} - 1 \right|^2}{K^2} \mathbb{E} \left[\left\| \mathbf{g}_k^{(t)} \right\|^2 \right] + \frac{\sigma_z^2}{K^2} \\ &\leq \frac{\sum_k \left| (\mathbf{m}^{(t)})^H \tilde{\mathbf{h}}_k^{(t)} b_k^{(t)} - 1 \right|^2}{K^2} \left(\gamma_1 + \frac{\sigma^2}{BK^2} \right) + \frac{\sigma_z^2}{K^2}. \quad (46) \end{aligned}$$

Hence we can obtain the optimality gap in Theorem 1 by replacing the relevant terms in (44).

APPENDIX B: PROOF OF THEOREM 2

Without loss of generality, we adopt the quadratic Lyapunov function $L(\mathbf{e}(t)) \triangleq \frac{1}{2} \sum_{k \in \mathcal{K}} e_k^2(t)$. Besides the 1-round Lyapunov drift and the R -round Lyapunov drift are represented as $\Delta_1(t) \triangleq L(\mathbf{e}(t+1)) - L(\mathbf{e}(t))$ and $\Delta_R(t) \triangleq L(\mathbf{e}(t+R)) - L(\mathbf{e}(t))$, respectively. According to (20), we have

$$\begin{aligned} \frac{1}{2} \sum_{k \in \mathcal{K}} e_k^2(t+1) &\leq \frac{1}{2} \sum_{k \in \mathcal{K}} \left(\tilde{\gamma} |b_k^{(t)}|^2 / d - P_k^{\text{avg}} + e_k(t) \right)^2 \\ &\leq C_e + \frac{1}{2} \sum_{k \in \mathcal{K}} e_k^2(t) + \sum_{k \in \mathcal{K}} e_k(t) \left(\tilde{\gamma} |b_k^{(t)}|^2 / d - P_k^{\text{avg}} \right), \quad (47) \end{aligned}$$

where $C_e = \frac{1}{2} K E_{\max}^2$ with $E_{\max} = \max_{k,t} (\tilde{\gamma} |b_k^{(t)}|^2 / d - P_k^{\text{avg}})$. Thus,

$$\begin{aligned} \Delta_1(t) &\leq C_e + \sum_{k \in \mathcal{K}} e_k(t) \left(\tilde{\gamma} |b_k^{(t)}|^2 / d - P_k^{\text{avg}} \right) \\ &\leq C_e + \sum_{k \in \mathcal{K}} e_k(t) (P_k^{\max} - P_k^{\text{avg}}). \quad (48) \end{aligned}$$

For arbitrary r -th period with V_r , we have

$$\begin{aligned} & \Delta_R^\dagger(r\rho) + V_r \sum_{t=r\rho+1}^{(r+1)\rho} G_t^\dagger \\ &\leq \rho C_e + \sum_{t=r\rho+1}^{(r+1)\rho} \sum_{k \in \mathcal{K}} e_k(t) \left(\tilde{\gamma} |b_k^{(t)}|^2 / d - P_k^{\text{avg}} \right) + V_r \sum_{t=r\rho+1}^{(r+1)\rho} G_t^* \\ &\leq \rho C_e + \sum_{t=r\rho+1}^{(r+1)\rho} \sum_{k \in \mathcal{K}} E_{\max} ((t-1)E_{\max} + e_k(r\rho+1)) \\ &\quad + V_r \sum_{t=r\rho+1}^{(r+1)\rho} G_t^*. \quad (49) \end{aligned}$$

Note that $\Delta_R^\dagger(r\rho) \geq 0$, thus

$$\sum_{t=r\rho+1}^{(r+1)\rho} G_t^\dagger \leq \sum_{t=r\rho+1}^{(r+1)\rho} G_t^* + \frac{C_r}{V_r}, \quad (50)$$

where $C_r = \rho C_e + \sum_{t=r\rho+1}^{(r+1)\rho} \sum_{k \in \mathcal{K}} E_{\max} ((t-1)E_{\max} + e_k(r\rho+1))$. Summing over all the R periods, we can obtain

$$\sum_{t=1}^T G_t^\dagger \leq \sum_{t=1}^T G_t^* + \sum_{r=1}^{R-1} \frac{C_r}{V_r}. \quad (51)$$

Note that

$$\Delta_R(t) \triangleq L(\mathbf{e}(t+R)) - L(\mathbf{e}(t)) = \sum_k \frac{1}{2} e_k^2(R+1). \quad (52)$$

Hence, we have

$$\begin{aligned} & \sum_{t=r\rho+1}^{(r+1)\rho} \left(\tilde{\gamma} |b_k^{(t)}|^2 / d - P_k^{\text{avg}} \right) \leq \sum_{t=r\rho+1}^{(r+1)\rho} (e_k(t+1) - e_k(t)) \\ &= e_k((r+1)\rho+1) - e_k(r\rho+1) \leq \sqrt{2\Delta_\rho} - e_k(r\rho+1) \\ &\leq \sqrt{2 \left(C_r + V_r \sum_{t=r\rho+1}^{(r+1)\rho} G_t^* \right)} - e_k(r\rho+1). \quad (53) \end{aligned}$$

Summing over all the R periods, we can obtain the (23) in Theorem 2.

REFERENCES

- [1] G. Zhu, D. Liu, Y. Du, C. You, J. Zhang, and K. Huang, "Toward an intelligent edge: Wireless communication meets machine learning," *IEEE Commun. Mag.*, vol. 58, no. 1, pp. 19–25, Jan. 2020.
- [2] K. B. Letaief, Y. Shi, J. Lu, and J. Lu, "Edge artificial intelligence for 6g: Vision, enabling technologies, and applications," *IEEE J. Sel. Areas Commun.*, vol. 40, no. 1, pp. 5–36, Jan. 2022.
- [3] Y. Shi, K. Yang, T. Jiang, J. Zhang, and K. B. Letaief, "Communication-efficient edge AI: algorithms and systems," *IEEE Commun. Surv. Tutorials*, vol. 22, no. 4, pp. 2167–2191, 4th Quat., 2020.
- [4] W. Y. B. Lim, N. C. Luong, D. T. Hoang, Y. Jiao, Y. Liang, Q. Yang, D. Niyato, and C. Miao, "Federated learning in mobile edge networks: A comprehensive survey," *IEEE Commun. Surv. Tutorials*, vol. 22, no. 3, pp. 2031–2063, 3th Quat., 2020.
- [5] S. A. Rahman, H. Tout, H. Ould-Slimane, A. Mourad, C. Talhi, and M. Guizani, "A survey on federated learning: The journey from centralized to distributed on-site learning and beyond," *IEEE Internet Things J.*, vol. 8, no. 7, pp. 5476–5497, Oct. 2021.
- [6] M. Chen, D. Gündüz, K. Huang, W. Saad, M. Bennis, A. V. Feljan, and H. V. Poor, "Distributed learning in wireless networks: Recent progress and future challenges," *IEEE J. Sel. Areas Commun.*, vol. 39, no. 12, pp. 3579–3605, Oct. 2021.
- [7] S. Wang, M. Lee, S. Hosseinalipour, R. Morabito, M. Chiang, and C. G. Brinton, "Device sampling for heterogeneous federated learning: Theory, algorithms, and implementation," in *IEEE Conference on Computer Communications, (INFOCOM), Vancouver, BC, Canada, May 2021*, pp. 1–10.
- [8] E. Ozfatura, K. Ozfatura, and D. Gündüz, "Time-correlated sparsification for communication-efficient federated learning," in *Proc. IEEE Int. Symp. Inf. Theory (ISIT)*, Melbourne, Australia, July 2021, pp. 461–466.
- [9] D. Alistarh, D. Grubic, J. Li, R. Tomioka, and M. Vojnovic, "QSGD: communication-efficient SGD via gradient quantization and encoding," in *Proc. Neural Inf. Process. Syst. (NeurIPS)*, Long Beach, CA, USA, Dec. 2017, pp. 1709–1720.
- [10] J. Bernstein, Y. Wang, K. Azizzadenesheli, and A. Anandkumar, "SIGNSGD: compressed optimisation for non-convex problems," in *Proc. Int. Conf. Mach. Learn. (ICML)*, Stockholm, Sweden, July 2018, pp. 559–568.
- [11] K. Yang, T. Jiang, Y. Shi, and Z. Ding, "Federated learning via over-the-air computation," *IEEE Trans. Wirel. Commun.*, vol. 19, no. 3, pp. 2022–2035, Jan. 2020.
- [12] G. Zhu, J. Xu, K. Huang, and S. Cui, "Over-the-air computing for wireless data aggregation in massive IoT," *IEEE Wirel. Commun.*, vol. 28, no. 4, pp. 57–65, Aug. 2021.
- [13] A. Giridhar and P. R. Kumar, "Computing and communicating functions over sensor networks," *IEEE J. Sel. Areas Commun.*, vol. 23, no. 4, pp. 755–764, Apr. 2005.

- [14] B. Nazer and M. Gastpar, "Computation over multiple-access channels," *IEEE Trans. Inf. Theory*, vol. 53, no. 10, pp. 3498–3516, Sept. 2007.
- [15] —, "Compute-and-forward: Harnessing interference through structured codes," *IEEE Trans. Inf. Theory*, vol. 57, no. 10, pp. 6463–6486, Oct. 2011.
- [16] M. Goldenbaum, H. Boche, and S. Stanczak, "Analyzing the space of functions analog-computable via wireless multiple-access channels," in *Proc. IEEE Int. Symp. Wireless Commun. Syst. (ISWCS)*, Aachen, Germany, Nov. 2011, pp. 779–783.
- [17] —, "Harnessing interference for analog function computation in wireless sensor networks," *IEEE Trans. Signal Process.*, vol. 61, no. 20, pp. 4893–4906, Oct. 2013.
- [18] M. Goldenbaum, S. Stanczak, and H. Boche, "On achievable rates for analog computing real-valued functions over the wireless channel," in *Proc. IEEE Int. Conf. Commun. (ICC)*, London, United Kingdom, June 2015, pp. 4036–4041.
- [19] G. Zhu and K. Huang, "MIMO over-the-air computation for high-mobility multimodal sensing," *IEEE Internet Things J.*, vol. 6, no. 4, pp. 6089–6103, Aug. 2019.
- [20] M. Fu, Y. Zhou, Y. Shi, W. Chen, and R. Zhang, "UAV aided over-the-air computation," *IEEE Trans. Wireless Commun.*, 2021, Early Access, doi: 10.1109/TWC.2021.3134327.
- [21] U. Altun, S. T. Başaran, H. Alakoca, and G. K. Kurt, "A testbed based verification of joint communication and computation systems," in *Proc. IEEE Telecommun. Forum (TELFOR)*, Belgrade, Serbia, Jan. 2017, pp. 1–4.
- [22] H. Guo, Y. Zhu, H. Ma, V. K. N. Lau, K. Huang, X. Li, H. Nong, and M. Zhou, "Over-the-air aggregation for federated learning: Waveform superposition and prototype validation," *J. Commun. Inf. Networks*, vol. 6, no. 4, pp. 429–442, Dec. 2021.
- [23] M. Chen, H. V. Poor, W. Saad, and S. Cui, "Convergence time optimization for federated learning over wireless networks," *IEEE Trans. Wirel. Commun.*, vol. 20, no. 4, pp. 2457–2471, Apr. 2021.
- [24] Z. Yang, M. Chen, W. Saad, C. S. Hong, and M. Shikh-Bahaei, "Energy efficient federated learning over wireless communication networks," *IEEE Trans. Wirel. Commun.*, vol. 20, no. 3, pp. 1935–1949, Mar. 2021.
- [25] J. Ren, Y. He, D. Wen, G. Yu, K. Huang, and D. Guo, "Scheduling for cellular federated edge learning with importance and channel awareness," *IEEE Trans. Wirel. Commun.*, vol. 19, no. 11, pp. 7690–7703, Nov. 2020.
- [26] Y. Sun, S. Zhou, Z. Niu, and D. Gündüz, "Dynamic scheduling for over-the-air federated edge learning with energy constraints," *IEEE J. Sel. Areas Commun.*, vol. 40, no. 1, pp. 227–242, Nov. 2022.
- [27] Z. Wang, J. Qiu, Y. Zhou, Y. Shi, L. Fu, W. Chen, and K. B. Letaief, "Federated learning via intelligent reflecting surface," *IEEE Trans. Wirel. Commun.*, vol. 21, no. 2, pp. 808–822, July 2022.
- [28] X. Wei and C. Shen, "Federated learning over noisy channels: Convergence analysis and design examples," *IEEE Trans. Cognit. Commun. Networking*, 2022, early access, doi:10.1109/TCCN.2022.3140788.
- [29] X. Cao, G. Zhu, J. Xu, Z. Wang, and S. Cui, "Optimized power control design for over-the-air federated edge learning," *IEEE J. Sel. Areas Commun.*, vol. 40, no. 1, pp. 342–358, Jan. 2022.
- [30] M. M. Amiri and D. Gündüz, "Machine learning at the wireless edge: Distributed stochastic gradient descent over-the-air," *IEEE Trans. Signal Process.*, vol. 68, pp. 2155–2169, Mar. 2020.
- [31] G. Zhu, Y. Du, D. Gündüz, and K. Huang, "One-bit over-the-air aggregation for communication-efficient federated edge learning: Design and convergence analysis," *IEEE Trans. Wirel. Commun.*, vol. 20, no. 3, pp. 2120–2135, Nov. 2021.
- [32] C. Xu, S. Liu, Z. Yang, Y. Huang, and K. Wong, "Learning rate optimization for federated learning exploiting over-the-air computation," *IEEE J. Sel. Areas Commun.*, vol. 39, no. 12, pp. 3742–3756, Dec. 2021.
- [33] J. Ren, G. Yu, and G. Ding, "Accelerating DNN training in wireless federated edge learning systems," *IEEE J. Sel. Areas Commun.*, vol. 39, no. 1, pp. 219–232, Jan. 2021.
- [34] Q. Wu, S. Zhang, B. Zheng, C. You, and R. Zhang, "Intelligent reflecting surface-aided wireless communications: A tutorial," *IEEE Trans. Commun.*, vol. 69, no. 5, pp. 3313–3351, Jan. 2021.
- [35] S. Gong, X. Lu, D. T. Hoang, D. Niyato, L. Shu, D. I. Kim, and Y. Liang, "Toward smart wireless communications via intelligent reflecting surfaces: A contemporary survey," *IEEE Commun. Surv. Tutorials*, vol. 22, no. 4, pp. 2283–2314, 4th Quart. 2020.
- [36] N. Rajatheva, I. Atzeni, S. Bicaïs, E. Björnson, A. Bourdoux, S. Buzzi, C. D'Andrea, J.-B. Dore, S. Erkucuk, M. Fuentes *et al.*, "Scoring the terabit/s goal: Broadband connectivity in 6g," 2020. [Online]. Available: <http://arxiv.org/abs/2008.07220>
- [37] M. Hua, Q. Wu, D. W. K. Ng, J. Zhao, and L. Yang, "Intelligent reflecting surface-aided joint processing coordinated multipoint transmission," *IEEE Trans. Commun.*, vol. 69, no. 3, pp. 1650–1665, Mar. 2021.
- [38] H. Liu, X. Yuan, and Y. A. Zhang, "Reconfigurable intelligent surface enabled federated learning: A unified communication-learning design approach," *IEEE Trans. Wirel. Commun.*, vol. 20, no. 11, pp. 7595–7609, June 2021.
- [39] W. Ni, Y. Liu, Z. Yang, H. Tian, and X. Shen, "Federated learning in multi-RIS aided systems," *IEEE Internet Things J.*, 2021, early access, doi: 10.1109/JIOT.2021.3130444.
- [40] J. Xu and H. Wang, "Client selection and bandwidth allocation in wireless federated learning networks: A long-term perspective," *IEEE Trans. Wirel. Commun.*, vol. 20, no. 2, pp. 1188–1200, Feb. 2021.
- [41] C. Shen, J. Xu, S. Zheng, and X. Chen, "Resource rationing for wireless federated learning: Concept, benefits, and challenges," *IEEE Commun. Mag.*, vol. 59, no. 5, pp. 82–87, May 2021.
- [42] Y. LeCun, L. Bottou, Y. Bengio, and P. Haffner, "Gradient-based learning applied to document recognition," *Proc. IEEE*, vol. 86, no. 11, pp. 2278–2324, Nov. 1998.
- [43] Q. Wu and R. Zhang, "Intelligent reflecting surface enhanced wireless network via joint active and passive beamforming," *IEEE Trans. Wirel. Commun.*, vol. 18, no. 11, pp. 5394–5409, Aug. 2019.
- [44] X. Lu, W. Yang, X. Guan, Q. Wu, and Y. Cai, "Robust and secure beamforming for intelligent reflecting surface aided mmwave MISO systems," *IEEE Wirel. Commun. Lett.*, vol. 9, no. 12, pp. 2068–2072, Dec. 2020.
- [45] M. P. Friedlander and M. Schmidt, "Hybrid deterministic-stochastic methods for data fitting," *SIAM J. Sci. Comput.*, vol. 34, no. 3, 2012.
- [46] L. Bottou, F. E. Curtis, and J. Nocedal, "Optimization methods for large-scale machine learning," *SIAM Rev.*, vol. 60, no. 2, pp. 223–311, 2018.
- [47] J. Wang and G. Joshi, "Cooperative SGD: A unified framework for the design and analysis of local-update SGD algorithms," *J. Mach. Learn. Res.*, vol. 22, no. 213, pp. 1–50, 2021.
- [48] H. Karimi, J. Nutini, and M. Schmidt, "Linear convergence of gradient and proximal-gradient methods under the polyak-lojasiewicz condition," in *Proc. Mach. Learn. and Knowledge Discovery in Databases (ECML PKDD)*, Riva del Garda, Italy, 2016, pp. 795–811.
- [49] H. Yu, S. Yang, and S. Zhu, "Parallel restarted SGD with faster convergence and less communication: Demystifying why model averaging works for deep learning," in *Proc. Conference on Artif. Intell. (AAAI)*, Honolulu, Hawaii, USA, July 2019, pp. 5693–5700.
- [50] A. Kulkarni, A. Seetharam, A. Ramesh, and J. D. Herath, "Deepchannel: Wireless channel quality prediction using deep learning," *IEEE Trans. Veh. Technol.*, vol. 69, no. 1, pp. 443–456, Jan. 2020.
- [51] M. Zhao, Q. Wu, M. Zhao, and R. Zhang, "Exploiting amplitude control in intelligent reflecting surface aided wireless communication with imperfect CSI," *IEEE Trans. Commun.*, vol. 69, no. 6, pp. 4216–4231, June 2021.
- [52] Z. Luo, W. Ma, A. M. So, Y. Ye, and S. Zhang, "Semidefinite relaxation of quadratic optimization problems," *IEEE Signal Process. Mag.*, vol. 27, no. 3, pp. 20–34, May 2010.
- [53] Q. Wu and R. Zhang, "Beamforming optimization for wireless network aided by intelligent reflecting surface with discrete phase shifts," *IEEE Trans. Commun.*, vol. 68, no. 3, pp. 1838–1851, Mar. 2020.
- [54] M. M. Amiri, D. Gündüz, S. R. Kulkarni, and H. V. Poor, "Convergence of federated learning over a noisy downlink," *IEEE Trans. Wirel. Commun.*, vol. 21, no. 3, pp. 1422–1437, Mar. 2022.